Entropy generation for forced convection in a porous channel with isoflux or isothermal walls

K. Hooman[1], F. Hooman[2], S.R. Mohebpour[3]

[1]*School of Engineering, The University of Queensland, Brisbane, Australia*

[2]*Chemical Engineering Faculty, Sharif University of Technology, Tehran, Iran*

[3]*Mechnical Engineering Department, Persian Gulf University, Bushehr, Iran*

and

[3]*School of Engineering, Islamic Azad University of Bushehr, Bushehr, Iran*

Abstract

A numerical study is reported to investigate the entropy generation due to forced convection in a parallel plate channel filled by a saturated porous medium. Two different thermal boundary conditions are considered being isoflux and isothermal walls. Effects of the Péclet number, the porous medium shape factor, the dimensionless temperature difference for isothermal walls, the dimensionless heat flux for isoflux walls, and the Brinkman number on the Bejan number as well as the local and average dimensionless entropy generation rate are examined.

Key words: forced convection, channel, entropy generation, irreversibility, Bejan number

Nomenclature

A area

a channel aspect ratio H/L

Be Bejan number

Br Darcy-Brinkman number $\frac{\mu U^2 H^2}{k(T_i - T_w)K}$ for **T** and $\frac{\mu U^2 H}{q'' K}$ for **H**

Br' clear fluid Brinkman number Br/S^2

C_F Forchheimer coefficient

c_P specific heat at constant pressure

FFI fluid friction irreversibility

H half channel width

HTI heat transfer irreversibility

k porous medium thermal conductivity

K permeability

L channel length

*Ns** Area-weighted average of Ns

Ns Entropy generation number

Nu Nusselt number

*P** pressure

p dimensionless pressure

Pe the Péclet number $\frac{2\rho c_p UH}{k}$

q'' wall heat flux

q^* dimensionless heat flux

Re^* $2\rho UH / \mu$

Re modified Reynolds number, Re^*/ε^2

S the shape factor $H/\sqrt{K}$

$\dot{S}_{gen}$ Entropy generation rate per unit volume

T^* dimensionless temperature difference

T temperature

T_{in} Fluid inlet temperature

T_w wall temperature

u^* x-velocity

u u*/U

U inlet velocity

v* y-velocity

v v*/U

x^* longitudinal coordinate

x x*/H

y^* transverse coordinate

y y^*/H

Greek symbols

ε porosity

θ dimensionless temperature

θ_b dimensionless bulk temperature

μ fluid viscosity

ρ fluid density

ψ dimensionless stream function

ϕ dimensionless viscous dissipation function

ϕ^* viscous dissipation function, $\phi^* = \phi U^2 / K$

ω dimensionless vorticity

Ω temperature ratio equal to $(T_{in}-T_w)/ T_w$ ($q^* = q'' H /(kT_{in})$ for **T (H)** case

1. Introduction

Analysis of forced convection in parallel plate channels saturated with porous medium has been a subject of fundamental importance for being relevant to a lot of industrial applications including thermal insulation, solid matrix heat exchangers, and microelectronic heat transfer equipment as noted by Nield and Bejan (2006) or Bejan et al. (2004). However, a quick search of the literature shows that the Second Law (of Thermodynamics) aspects of non-Darcy forced convection through a parallel plate channel has not been analyzed when the hydrodynamic or thermal boundary layers are still to develop which is the subject of this study. On the other hand, a great deal of information is available dealing with the Second Law analysis of similar problems. Abu-Hijleh (2002) has reported a numerical analysis of entropy generation for cross-flow heat transfer from a cylinder covered with a porous layer. Mahmud and Fraser (2003) have analytically reported the Second Law analysis of fundamental convective heat transfer problems. Later, Mahmud and Fraser (2004) extended their previous work to a steady state conjugate problem. Baytas (2004) has reported an interesting analysis of entropy generation for both natural and forced convection in a porous medium. Hooman (2005-a,b) has analytically investigated entropy generation for slug flow forced convection through ducts of circular and elliptical cross-section for the case when viscous dissipation effects are significant. Another analysis of irreversibility has been reported by Hooman and Gurgenci (2007-a) for fully developed slug flow through a porous duct of rectangular cross-section. Applying the Brinkman flow model, Hooman and Ejlali (2006) dealt with entropy production for thermally developing forced convection in a porous tube with the effects of viscous dissipation being included. Hooman (2006) has presented a theoretical

analysis of quasi-fully developed forced convection of a fluid with temperature-dependent viscosity through a circular porous-saturated tube. Available in that study was an analysis of the local entropy generation rate and the Bejan number. The work was different from that of Sahin (1998) where the author has analyzed cross-sectional averaged entropy generation for a similar problem through a non-porous circular tube. In an interesting study, Liu and Narusawa (2006) have applied the Brinkman flow model to examine the entropy generation for flow over the endothelial cell.

For an engineering (real) system the generated entropy is proportional to the destroyed exergy (which is always destroyed as a result of the Second Law; see Bejan (1982)). The destroyed exergy or the generated entropy is responsible for the less than maximum thermodynamic efficiency of a system which is associated with the reversible processes hypothesis. According to Bejan (1997), one can draw the map of exergy destruction distribution in a system by exergy accounting in smaller subsystems (total system $\rightarrow$ components $\rightarrow$ elemental surfaces $\rightarrow$ differential levels). Knowing the components that destroy the most exergy, one improves the efficiency by setting the optimized layout of the system in such a way that the minimum entropy be generated. This method, called entropy generation minimization (EGM), is a popular one among those who are interested in optimal design of applied systems for real life use.

In the view of the above, this study examines the entropy generation for forced convection through a porous medium bounded by two isothermal or isoflux parallel plates. A numerical simulation is conducted using the finite difference approximation. The resulting entropy generation rate and the Bejan number variations are investigated as a function of the effective system parameters.

2. Analysis

2.1 Basic equations: primitive variables

The fluid enters the channel at a uniform velocity/temperature being U/T_{in}. The channel is composed of two parallel plates $2H$ apart and each of them being held at either uniform temperature, T_w, or at uniform heat flux, q'', where the channel aspect ratio (defined as $a=L/H$) is fixed at a=8 which ensured us of the fully developed condition at the outlet. Figure 1 shows the schematic view of the problem under consideration. It is assumed that the magnitudes of the thermophysical properties are constant and that there is local thermal equilibrium. A criterion (that is met in most circumstances) for the validity of this assumption for steady forced convection was given by Nield (1998). Under these assumptions and by treating the solid matrix and the fluid as a continuum, the governing equations for uniform porosity distribution are

$$\nabla \vec{u}^* = 0, \tag{1}$$

$$\rho \vec{u}^*.\nabla \vec{u}^* = -\varepsilon^2 \nabla p^* + \varepsilon^2 \mu \nabla^2 \vec{u}^* - \varepsilon^2 \frac{\mu \vec{u}^*}{K} - \varepsilon^2 \frac{C_F \rho}{\sqrt{K}} \left|\vec{u}^*\right| .\vec{u}^*, \tag{2}$$

$$\rho c_p \vec{u}^*.\nabla T = k \nabla^2 T + \mu \phi^*. \tag{3}$$

Applying H, U, and $\rho U^2 \varepsilon^{-2}$ as scales of length, velocity, and pressure, respectively, the dimensionless form of the governing equations are obtained as

$$\nabla \vec{u} = 0, \tag{4}$$

$$\vec{u}.\nabla \vec{u} = -\nabla p + \frac{2}{\mathrm{Re}} \left(\nabla^2 \vec{u} - S^2 \vec{u}\right) - \Lambda |\vec{u}|.\vec{u}, \tag{5}$$

$$\vec{u}.\nabla \theta = \frac{2}{Pe} \left(\nabla^2 \theta + Br \phi\right), \tag{6}$$

Following Al-Hadhrami et al. (2003) the dimensionless viscous dissipation function, ϕ equal to $\phi = K\phi^* / U^2$, is defined as

$$\phi = u^2 + v^2 + \frac{1}{S^2}\left[2\left(\left(\frac{\partial u}{\partial x}\right)^2 + \left(\frac{\partial v}{\partial y}\right)^2\right) + \left(\frac{\partial v}{\partial x} + \frac{\partial u}{\partial y}\right)^2\right]. \quad (7)$$

Nield (2002) argued that when non-Darcian effects are important, which is the case here; the Darcy dissipation term should not be neglected compared to the clear-fluid compatible term in the thermal energy equation. Consequently, Hooman and Ejlali (2005) and Hooman et al. (2007a-c) have retained both the Darcy dissipation term (the velocity square term) and the clear-fluid compatible term in the entropy generation expression. However, there are some papers where the authors have neglected the Darcy term and, in view of the above, this will lead to incorrect modeling of viscous dissipation (and as a result the fluid friction irreversibility term). It is worth noting that there are three alternative models for viscous dissipation in a porous medium. Recently, Hooman and Gurgenci (2007-b) have compared these models for flow through a porous-saturated duct and concluded that for small Darcy numbers the three alternatives are effectively the same while for the high Darcy limits, i.e. the clear fluid problem, the only appropriate model is that of Al-Hadhrami et al. (2003). For more details on the alternative viscous dissipation models for flow through a porous media one may consult Nield (2000),(2002),(2004),(2006), Nield and Hooman (2006), Nield et al. (2003), (2004) and Magyari et al. (2005). The dimensionless temperature profile for **T** and **H** boundary conditions are $\theta = \frac{T - T_w}{T_{in} - T_w}$ and $\theta = k\frac{T - T_{in}}{q''H}$, respectively. Other dimensionless parameters are defined in the nomenclature so that the definitions are not repeated here.

According to Bejan (1982), one can find the volumetric entropy generation rate as

$$\dot{S}_{gen} = HTI + FFI \,, \tag{8-a}$$

where *HTI* is the heat transfer irreversibility due to heat transfer in the direction of finite temperature gradients. *HTI* is common in all types of thermal engineering applications. The last term (*FFI*) is the contribution of fluid friction irreversibility to the total entropy generation. Not only the wall and fluid layer shear stress (like the case of fluid clear of solid materials) but also the momentum exchange at the solid boundaries (pore level) contributes to *FFI*.

In terms of the primitive variables, *HTI* and *FFI* become

$$HTI = k\frac{\nabla T.\nabla T}{T^2}, \qquad FFI = \frac{\mu\phi^*}{T}. \tag{8-b,c}$$

where *T* is measured in degrees of Kelvin.

One can also define the Bejan number, *Be*, as

$$Be = \frac{HTI}{HTI + FFI}\,. \tag{9}$$

The Bejan number shows the ratio of entropy generation due to heat transfer irreversibility to the total entropy generation so that a *Be* value more/less than 0.5 shows that the contribution of *HTI* to the total entropy generation is higher/less than that of *FFI*. The limiting value of *Be*=1 shows that the only active entropy generation mechanism is *HTI* while a *Be*=0 value represents no *HTI* contribution to the total entropy production.

The dimensionless form of entropy generation rate, *Ns*, is defined as

$$Ns = \frac{\dot{S}_{gen}}{k}\left(\frac{H}{\Omega}\right)^2, \tag{10}$$

one finds that

$$Ns = \frac{\left(\frac{\partial\theta}{\partial x}\right)^2 + \left(\frac{\partial\theta}{\partial y}\right)^2}{\left(1+\Omega\theta\right)^2} + Br^* \frac{u^2+v^2+S^{-2}\left(2\left(\left(\frac{\partial u}{\partial x}\right)^2+\left(\frac{\partial v}{\partial y}\right)^2\right)+\left(\frac{\partial v}{\partial x}+\frac{\partial u}{\partial y}\right)^2\right)}{\left(1+\Omega\theta\right)}, \quad (11)$$

where the modified Darcy-Brinkman number, *Br**, is defined as

$$Br^* = \frac{Br}{\Omega}. \quad (12)$$

Moreover, the dimensionless heat flux (*q**) and the dimensionless temperature difference (*T**) are defined for **H** and **T** boundary condition as

$$q^* = \frac{q''H}{kT_{in}}, \qquad T^* = \frac{T_{in}-T_w}{T_w}. \quad (13\text{-a,b})$$

In equations (10-12) Ω will be replaced by *T** or *q** for **T** or **H** boundary conditions, respectively.

The area-weighted average for *Ns* is defined as

$$Ns^* = \frac{\int_A Ns dA}{A} \quad (14\text{-a})$$

where, based on the dimensionless duct size (1x8 box) shown in figure 1, equation (14-a) reads

$$Ns^* = \frac{\int_0^1\int_0^8 Ns dx dy}{8}. \quad (14\text{-b})$$

2.2 Methodology

The vorticity-stream function method is applied to solve the set of equations (4-7). Taking the curl of the momentum equations in *x* and *y* direction, one finds that

$$\frac{\partial(u\omega)}{\partial x}+\frac{\partial(v\omega)}{\partial y}=\frac{2}{\mathrm{Re}}\left(\frac{\partial^2\omega}{\partial x^2}+\frac{\partial^2\omega}{\partial y^2}-S^2\omega\right), \tag{15}$$

where

$$\omega=-\left(\frac{\partial^2\psi}{\partial x^2}+\frac{\partial^2\psi}{\partial y^2}\right), \tag{16}$$

is the vorticity directed in *z* direction and the stream function, ψ, is defined as

$$u=\frac{\partial\psi}{\partial y},\qquad v=-\frac{\partial\psi}{\partial x}. \tag{17-a,b}$$

One knows that in this way the continuity equation is satisfied identically.

The thermal energy equation now takes the following form

$$\frac{\partial(u\theta)}{\partial x}+\frac{\partial(v\theta)}{\partial y}=\frac{2}{Pe}\left(\frac{\partial^2\theta}{\partial x^2}+\frac{\partial^2\theta}{\partial y^2}+Br\phi\right). \tag{18}$$

Note that the clear fluid Brinkman number Br' is related to our Darcy-Brinkman number as $Br'=BrS^{-2}$.

The appropriate set of boundary conditions is shown in figure 1. More details of the vorticity-stream function method may be found in Bejan (1984).

Following Nield and Bejan (2006), the Nusselt number is defined in terms of the channel width rather than the hydraulic diameter, for **T** and **H** cases as

$$Nu_T=\frac{-2\left.\frac{\partial\theta}{\partial y}\right|_{y=0}}{\theta_b},\qquad Nu_H=\frac{2}{\theta_w-\theta_b}, \tag{19-a,b}$$

wherein the dimensionless bulk mean temperature, independent of the boundary condition, is defined as

$$\theta_b = \int_0^1 u\theta dy \,. \tag{20}$$

Applying Ψ and ω to equation (11), one finds local *Ns* and *Be* as

$$Ns = \frac{(\nabla\theta)^2}{(1+\Omega\theta)^2} + Br^* \frac{(\nabla\psi)^2 + S^{-2}\left((2\frac{\partial^2\psi}{\partial y\partial x})^2 + \omega^2\right)}{(1+\Omega\theta)},$$
$$Be = \frac{(\nabla\theta)^2}{(\nabla\theta)^2 + Br^*(1+\Omega\theta)\left((\nabla\psi)^2 + S^{-2}\left((2\frac{\partial^2\psi}{\partial y\partial x})^2 + \omega^2\right)\right)}. \tag{21-a,b}$$

3. Numerical details

In this study the computational domain is chosen to be larger than the physical one to eliminate the entrance and exit effects. The computational domain is symmetric above the horizontal mid-plane and therefore the lower half of the flow region is considered, as shown in figure 1-b, to reduce the computational time. Numerical solution for the governing equations for vorticity, stream function, and dimensionless temperature are obtained by finite difference methods, using the Gauss-Seidel technique with SOR. The governing equations are discretized by applying the second-order accurate central difference schemes. For the numerical integration, algorithms based on the trapezoidal rule, similar to Hooman (2007), are employed.

All runs were performed with a 30 x 200 grid. Grid independence was verified by running different combinations of *S, Re, Br,* and *Pe* on a 60 x 400 grid for both boundary conditions to observe that the results will not change to four significant figures. The convergence criterion (maximum relative error in the values of the dependent variables

between two successive iterations) in all test runs was set at 10^{-6}. Accuracy of the numerical procedure was verified by comparison of the results given in the literature, as shown in tables 1 and 2.

Table 1 verifies our numerical results by recovering the exact solution presented for **T** boundary condition in Nield et al. (2003) and Haji-Sheikh et al. (2004) while table 2 compares our results with those of Nield et al. (2004) reported for **H** boundary condition. It is worth noting that for very high S values ($S \to \infty$), with a non-zero Br, for both boundary conditions our Nu tends to 6. For **T** boundary condition it is in complete agreement with that of Hooman and Gorji-Bandpy (2005) and confirms Nu=5.953 reported by Nield et al. (2003). Also for **H** boundary condition our Nu agrees well with that of Nield and Bejan (2006) and Haji-Sheikh et al. (2006).

4. Results

In this problem there is a large number of parameters to vary and it would be a very spacious task to show the First Law aspects of the problem so that, for the sake of brevity, just the Second Law results will be reported in terms of Be, Ns, and Ns*. Though the contour maps could have been shown, for an effective investigation of the problem, Ns and Be are illustrated in figures (2-7) versus the transverse coordinate at some streamwise locations. To complete the picture, figures (8-9) are presented to show the area-weighted results of Ns versus effective system parameters. Figures (2-4) and figure 9, are presented for **H** boundary condition while figures (5-8) are for the **T** case. In all of the figures the following values are used unless otherwise noted Re=2, Pe=5, T*=0.1, and q*=0.1.

Moving from figure 2 to figure 4, the effects of *Br** on the Second Law aspects of the problem will be examined in such a way that each figure represents limiting *Br** compared to unity, i.e. 0.1, 1, and 10, respectively. Meanwhile, *S* is changed within eachfigure, in such a way that the first pair of the charts is pertaining to *S*=1 while for the second one it is *S*=10, to show the effects of a change in the porous media shape factor with a fixed *Br**. It is worth noting that this selection is based on the fact that *S*=1 represents a hyperporous medium case (see Nield and Bejan (2006) for more details) while, according to Hooman and Merrikh (2006) and Hooman and Gurgenci (2007-c), for *S*>10 the flow is more or less a slug-like one.

Before moving to the results, one should note that, generally speaking, high values of *Ns* are expected in the near wall regions due to the presence of severe velocity and temperature gradients (which in turn lead to very high values of *FFI* and *HTI*) compared to the centerline, where due to symmetry, both velocity and temperature gradients will vanish. Moving down the channel, the problem becomes hydrodynamically fully developed so that viscous dissipation function will not change with *x*, *i.e.* $\phi = u^2 + (\frac{du}{dy})^2 / S^2$. On the other hand, as fluid flows in the duct its (bulk) temperature gets closer to that of the wall and hence *HTI* will decrease with *x*. This, in turn, will decrease *Ns* along the channel.

Another feature of considerable interest is that, in all figures pertaining to *Be* or *Ns*, two different behaviors can be recognized. Plots of *x*=0.1 and *x*=0.5 behave similar to each other and different from those of higher *x* values (which are qualitatively identical to one another). This should be due to the fact that small values of *x* are associated with the

hydrodynamically developing region, see for example figure 5 of Hooman and Gurgenci (2007-b).

Figures 2-a,b are presented to show *Ns* and *Be* for *S*=1 while *S*=10 is assumed in obtaining figures 2-c,d. As shown by figure 2-a, for all streamwise locations *Ns* starts from a maximum at the wall and then plunges to its minimum at the channel centerline and moving down the channel, the difference between the two extremes decreases, as expected based on the general arguments presented above. Figure 2-b shows that *Be* starts from a minimum at the wall, where *Ns* reaches its maximum value, increases to a maximum and then decreases toward the channel centerline. Moving down the channel, this maximum becomes smaller in value and shifts to the half distance, say *y*=0.5, leading to a more flattened *Be* curve. *Be* is the ratio of *HTI* to total entropy generation, so that, to the first approximation, for uniform distribution of *HTI*, one can conclude that *Be* is inversely proportional to *Ns*. Note that though *HTI* is not uniform in *y*, to a good estimate, this argument explains why *Be* decreases with an increase in *Ns*. One should, however, be warned that *HTI* is not the only influential parameter on *Be* but *FFI/HTI* ratio or the irreversibility distribution ratio, in the terminology of Bejan (1982), which is a function of not only the local temperature and velocity but also of their gradients.

Examining figures 2-c,d, one observes that *Ns* plots show more or less the same trend as the previous case, however, for *Be* the situation completely differs in such a way that it starts from a relatively high value at the wall, increases to a maximum value near the wall and then decreases toward the channel center where at, *y*=1, *Be* increases slightly. This can be justified by noting that for such high values of *S* the clear fluid compatible part of the viscous dissipation function becomes negligible ($O(0.01)$) compared to the Darcy

dissipation term (velocity square term) leading to a decrease in *FFI*. This means that *HTI* is the dominant part of *Ns* as reflected in *Be* plots which are qualitatively similar to those of *Ns*. Moreover, *Be* puts on very high values (near unity which is the maximum possible value for *Be*) that confirms the dominant effect of *HTI* contribution to *Ns* over that of *FFI*.

Figure 3 is presented to show the effects of a change in *Br** on *Ns* and *Be*. This figure is quite similar to figure 2 with the only difference being a chagne in *Br*=0.1* to *Br*=1*. The trends observed in *Be* and *Ns* plots are qualitatively similar for both *Br** values, nevertheless, one observes a local minimum in *Ns* plots for *Br*=1* in addition to the least *Ns* value observed in the channel center. For *S=1* this local minimum is vanished downstream the channel while for *S=10*, excluding *x=0.1*, the local minimum happens at just under *y=0.1* where *Be* reaches its maximum value. This is again in line with our approximation-based argument on inverse proportionality of *Be-Ns*.

Figure 4 shows the case of *Br*=10* with the other parameters fixed at those used in the previous two figures. Near the duct entry, *Be* acts more or less similar to those of smaller *Br** while for large values of *x* the trend changes in such a way that *Be* starts from a minimum at the wall and then increases to reach a maximum at half way to the duct center where, after this point, the *Be* value remains approximately constant toward the axis of symmetry. Comparing the Bejan number plots with those of smaller *Br**, one observes that though qualitatively similar, the *Be* levels are different in such a way that higher *Br** values are associated with smaller *Be* levels and one expects that increasing *Br** confine high values of *Be* to *Be<0.5* which shows that the entropy generation happens more due to *FFI* than *HTI*. For *Ns* the plots are qualitatively similar to those of

Br=1* with the slight difference that near the exit cross-section *Ns* plots fall well below the local minimum of the near entrance cross-section.

Figure 5 shows the results for *Br*=1, S=1* when the boundary condition is an isothermal one, i.e. the **T** boundary condition. Comparing with figure 5-a, the trend observed in *Ns* is more or less similar to that of **H** boundary condition counterpart with the same *Br** and *S*. The Bejan number increases from the wall to a maximum and then plunges to its minimum value at *y*=1. It is interesting that moving down the channel, the trend of *Be* changes in such a way that *Be* decreases uniformly from the wall to the channel center so that the curves become flattened compared to smaller values of *x*. The reason is that far away from the duct inlet the problem becomes thermally fully developed. It means that for the isothermal walls the longitudinal temperature gradient vanishes while for the isoflux case it should take a constant value; see Nield (2006) or Hooman et al. (2006). One notes that vanishing the longitudinal temperature gradient will reduce *HTI*, and consequently *Be*, for the thermally fully developed region compared to the developing counterpart.

Figure 6 is presented to show how *Ns* and *Be* will change as *Br** increases from 1 to 10. As seen, for *x*=0.1 *Ns* experiences two minima while for *x*>0.5 *Ns* starts from its maximum at the wall, passes through a minimum and then increases toward the channel center. Moving down the channel, the minimum vanishes and *Ns* decreases from its maximum at the wall to its least value at the centerline. This can be attributed to the interaction between hydrodynamic development and the near-wall effects.

For this case, the Bejan number decreases from its maximum at the wall to a local minimum and then increases again at a short distance to a second local maximum where

after this value increases to the centerline for x=0.1. It is interesting that the second maximum in *Be* is associated with a transverse location where *Ns* experiences a minimum. For x=0.5, there exists just one minimum, excluding that of y=0, where moving down the channel, this minimum vanishes and the plots show a uniform decrease from the wall.

To show how a change in *S* and T* will alter the Second Law aspects of the problem, figure 7 is presented. Figure 7-a shows that *Ns* decreases form wall to the channel center. For small values of x the value of *Ns* becomes constant after a short distance from the wall (moving downstream the distance increases) but for large values of x, i.e. in the fully developed region, *Ns* values continue to decrease till the duct centerline at y=1.

According to figure 7-b, the *Be* plots are showing two different behavior for small and large x, i.e. for the developing and the fully developed region. For near entry region, *Be* decreases from the wall, passes through some local minima toward the channel centerline where the number of these minima decreases as the flow becomes fully developed in such a way that for very large values of x a uniform decrement is observed in *Be* from the wall to the duct center. It is interesting that, for y<0.25 in the fully developed region, *Be*>0.5 or *HTI*>*FFI* and for 0.25<y<1 the situation changes in such a way that *Be* <0.5, i.e. *HTI*<*FFI*. This fact drives home the point that this is not only *Br** that shows the relative importance of the contributing irreversibility sources but the heat transfer mechanism also affects the balance between *HTI* and *FFI*. In the asymptotic region the energy balance is a conduction-generation one as noted by previous investigators for similar problems. Here, heat generation is due to viscous dissipation which contributes to *FFI* while conduction leads to *HTI* and the First Law of thermodynamics proposes a balance

between generation-conduction while the Second Law can give clues of the corresponding exergy destruction mechanisms, i.e. *FFI* and *HTI*.

For figures 7-c,d with *S*=10, one observes that *Ns* patterns are almost unchanged while the plots of *Be* experience less ups and downs compared to those of *S*=1 but the trend is more or less similar.

Figure 8 shows average *Ns* value (*Ns**) versus the clear fluid Brinkman number for some *S* and *T** values when the boundary conditions are of **T** type. One observes that *Ns** increases with an increase in either the clear fluid Brinkman or the shape factor for an increase in *FFI*. On the contrary, increasing *T** decreases *Ns** through an increase in the denominator of both *HTI* and *FFI*.

Figure 9 shows *Ns** versus the clear fluid Brinkman number. As seen, like the **T** boundary condition, increasing either the porous media shape factor or the clear flow Brinkman number increases *Ns**, however, increasing *q** and *Pe* decreases *Ns** as both of them turn up in the denominator of *Ns*. No significant change in *Ns** plots is observed when *Re* was changed (from *Re*=1 to *Re*=10) for either of the two cases. It is worth noting that, with the other parameters fixed, a change in *S*, will alter the *Ns**-*Br'* slope. This fact is in line with the approximate solutions of *Ns**, reported by Hooman and Haji-Sheikh (2007), where it was concluded that for limiting (very small/high) values of *S*, *Ns** follows dissimilar functions of *Br'*.

5. Conclusion

The issue of entropy generation for forced convection in a parallel-plate channel filled with a porous medium has been studied both for uniform-temperature and uniform-flux

boundary conditions. The effect of various system parameters on the Second Law aspects of the problem has been investigated. It is observed that, regardless of the boundary condition, increasing the porous media shape factor and the Brinkman number, and decreasing the dimensionless heat flux or temperature difference, increases the dimensionless degree of irreversibility of the problem, as reflected in *Ns*. Moreover, one concludes that different arrangement of the parameters will lead to completely different behavior for both *Ns* and *Be* as described.

Acknowledgments

The first author, the scholarship holder, acknowledges the support provided by The University of Queensland in terms of UQILAS, Endeavor IPRS, and School Scholarship. The third author also acknowledges the financial support provided by Islamic Azad University of Bushehr.

Note added in proof. We are indebted to the reviewers for their improving suggestions.

References

Abu-Hijleh B.A. (2002) ‘Entropy generation due to cross-flow heat transfer from a cylinder covered with an orthotropic porous layer,’ *Heat Mass Transfer,* Vol. 39, pp. 27–40.

Al-Hadhrami A.K., Elliott L., Ingham D.B. (2003) ‘A new model for viscous dissipation in porous media across a range of permeability values,’ *Transport Porous Media*, Vol. 53, pp. 117-122.

Baytas A.C. (2004) 'Entropy generation for free and forced convection in a porous cavity and a porous channel,' in *Emerging Technology and Techniques in Porous Media* (Eds. D.B. Ingham et al.), Kluwer Academic Publishers, pp. 259-270.

Bejan A. (1982) *Entropy Generation through Heat and Fluid Flow*, New York, Wiley.

Bejan A. (1984) *Convection Heat Transfer*, New York, Wiley.

Bejan A. (1997) *Advanced engineering thermodynamics*, 2nd Ed., Wiley, New York.

Bejan A., Dincer I, Lorente S., Miguel A.F., Reis A.H. (2004) *Porous and complex flow structures in modern technology*, Springer-Verlag, New York.

Haji-Sheikh A., Minkowycz W.J., Sparrow E.M. (2004) 'Green's function solution of temperature field for flow in porous passages,' *Int. J. Heat Mass Transfer*, Vol. 47, pp. 4685-4695.

Haji-Sheikh A., Nield D.A., Hooman K. (2006) 'Heat transfer in the thermal entrance region for flow through rectangular porous passages,' *Int. J. Heat Mass Transfer*, Vol. 49, pp. 3004–3015

Hooman K. (2005-a) 'Fully developed temperature distribution in a porous saturated duct of elliptical cross-section, with viscous dissipation effects and entropy generation analysis,' *Heat Transfer Research*, Vol. 36, pp. 237-245.

Hooman K. (2005-b) 'Second law analysis of thermally developing forced convection in a porous medium,' *Heat Transfer Research*, Vol. 36, pp. 437-447.

Hooman K. (2006) 'Entropy-energy analysis of forced convection in a porous-saturated circular tube considering temperature-dependent viscosity effects,' *Int. J. Exergy*, Vol. 3, pp.436–451.

Hooman, K. (2007) 'A perturbation solution for forced convection in a porous saturated duct,' J. Comput. Appl. Math. (2006),doi: 10.1016/j.cam.2006.11.005

Hooman K., Ejlali A. (2005) 'Second law analysis of laminar flow in a channel filled with saturated porous media: a numerical solution,' *Entropy*, Vol. 7, pp. 300-307.

Hooman K., Ejlali A. (2006) 'Entropy generation for forced convection in a porous saturated circular tube with uniform wall temperature,' International Communications in Heat and Mass Transfer (2007), doi:10.1016/j.icheatmasstransfer.2006.10.008

Hooman K., Gorji-Bandpy M. (2005) 'Laminar dissipative flow in a porous channel bounded by isothermal parallel plates,' *Appl. Math. Mech.*, Vol. 26, pp. 578-593.

Hooman K., Gurgenci H. (2007-a) 'Effects of temperature-dependent viscosity variation on entropy generation, heat, and fluid flow through a porous-saturated duct of rectangular cross-section,' Appl. Math. Mech, Vol. 28, pp.69-78.

Hooman K., Gurgenci H., (2007-b) 'Effects of viscous dissipation and boundary conditions on forced convection in a channel occupied by a saturated porous medium,' Transport in Porous Media (2007), doi:10.1007/s11242-006-9049-4

Hooman K., Gurgenci H. (2007-c) 'A theoretical analysis of forced convection in a porous saturated circular tube: Brinkman-Forchheimer model,' Transport Porous Media (2007), doi: 10.1007/s11242-006-9074-3

Hooman K., Haji-Sheikh A. (2007) 'Analysis of heat transfer and entropy generation for a thermally developing Brinkman-Brinkman forced convection problem in a rectangular duct with isoflux walls,' Int. J. Heat Mass Transfer, in press.

Hooman K., Gurgenci H., Merrikh A.A., (2007-a) 'Heat transfer and entropy generation optimization of forced convection in a porous-saturated duct of rectangular cross-section,' Heat Mass Transfer (2007), doi:10.1016/j.ijheatmasstransfer.2006.11.015

Hooman K., Haji-Sheikh A., Nield D.A. (2007-b) 'Thermally developing Brinkman-Brinkman forced convection in rectangular ducts with isothermal walls,' Heat Mass Transfer (2007), doi:10.1016/j.ijheatmasstransfer.2007.01.011

Hooman K., Merrikh A.A., Ejlali A. (2007-c) 'Comments on "Flow, thermal, and entropy generation characteristics inside a porous channel with viscous dissipation" by S. Mahmud and R.A. Fraser,' [Int. J. Thermal Sciences 44 (2005) 21–32], International Journal of Thermal Sciences (2007), doi:10.1016/j.ijthermalsci.2007.01.001

Hooman K., Pourshaghaghy, A., Ejlali, A. (2006) 'Effects of viscous dissipation on thermally developing forced convection in a porous saturated circular tube with an isoflux wall,' App. Math. Mech., Vol. 27, pp. 617-626.

Liu H.D., Narusawa U. (2006) 'Endothelial surface reorganization: Effects of a porous surface layer,' *J. Porous Media*, Vol. 9, pp.93-107.

Magyari E., Rees D.A.S., Keller B., *Effect of viscous dissipation on the flow in fluid saturated porous media*, in Handbook of Porous Media (K. Vafai, ed.), 2nd ed., Taylor and Francis, New York, 2005, 373-407.

Mahmud S., Fraser R.A. (2003) 'The second law analysis in fundamental convective heat transfer problems,' *Int. J. Thermal Sciences*, Vol. 42, pp. 177-186.

Mahmud S., Fraser R.A. (2004) 'Entropy-energy analysis of porous stack: steady state conjugate problem,' *Int. J. Exergy*, Vol. 1, pp. 385-398.

Nield D.A. (1998) 'Effects of local thermal non-equilibrium in steady convective processes in a saturated porous medium: forced convection in a channel,' *J. Porous Media*, Vol. 1, pp. 181-186.

Nield D.A. (2000) 'Resolution of a paradox involving viscous dissipation and nonlinear drag in a porous medium,' *Transport in Porous Media*, Vol. 41, pp. 349-357.

Nield D.A. (2002) 'Modelling fluid flow in saturated porous media and at interfaces,' in *Transport Phenomena in Porous Media II* (D. B. Ingham and I. Pop, eds.), Elsevier Science, Oxford.

Nield D.A. (2004) 'Comments on 'A new model for viscous dissipation in porous media across a range of permeability values' by A.K. Al-Hadhrami, L. Elliot and D.B. Ingham,' *Transport Porous Media*, Vol. 55, pp. 253-254.

Nield D.A. (2006) 'A note on a Brinkman-Brinkman forced convection problem,' *Transport Porous Media*, Vol. 64, pp. 185-188.

Nield D.A., Bejan A. (2006) *Convection in Porous Media*, 3rd ed., New York, Springer.

Nield D.A., Hooman K. (2006) 'Comments on "Effects of viscous dissipation on the heat transfer in forced pipe flow. Part 1: both hydrodynamically and thermally fully developed flow, and Part 2: thermally developing flow" by O. Aydin,' *Energy Conv. Manag*., Vol. 47, pp. 3501-3503.

Nield D.A., Kuznetsov A.V., Xiong M. (2003) 'Thermally developing forced convection in a porous medium: parallel plate channel with walls at constant temperature, with longitudinal conduction and viscous dissipation effects,' *Int. J. Heat Mass Transfer*, Vol. 46, pp. 643-651

Nield D.A., Kuznetsov A.V., Xiong M. (2004) 'Effects of viscous dissipation and flow work on forced convection in a channel filled by a saturated porous medium,' *Transport Porous Media*, Vol. 56, pp. 351-367.

Sahin A.Z. (1998) 'Second law analysis of laminar viscous flow through a duct subjected to a constant wall temperature,' *ASME J. Heat Transfer*, Vol. 120, pp.76-83.

Table 1 The summary of the present and benchmark results for Nu (S=1).

Nu_T		Nield et al. (2003)		Haji-Sheikh et al. (2004)	
Br=0	$Br \neq 0$	Br=0	$Br \neq 0$	Br=0	$Br \neq 0$
3.803	6.647	3.802	6.641	3.801	6.649

Table 2 The summary of the present and benchmark results for Nu (S=1).

Parameter	Nu_H		Nield et al. (2004)	
Br	0	1	0	1
Nu	3.803	6.647	3.802	6.641

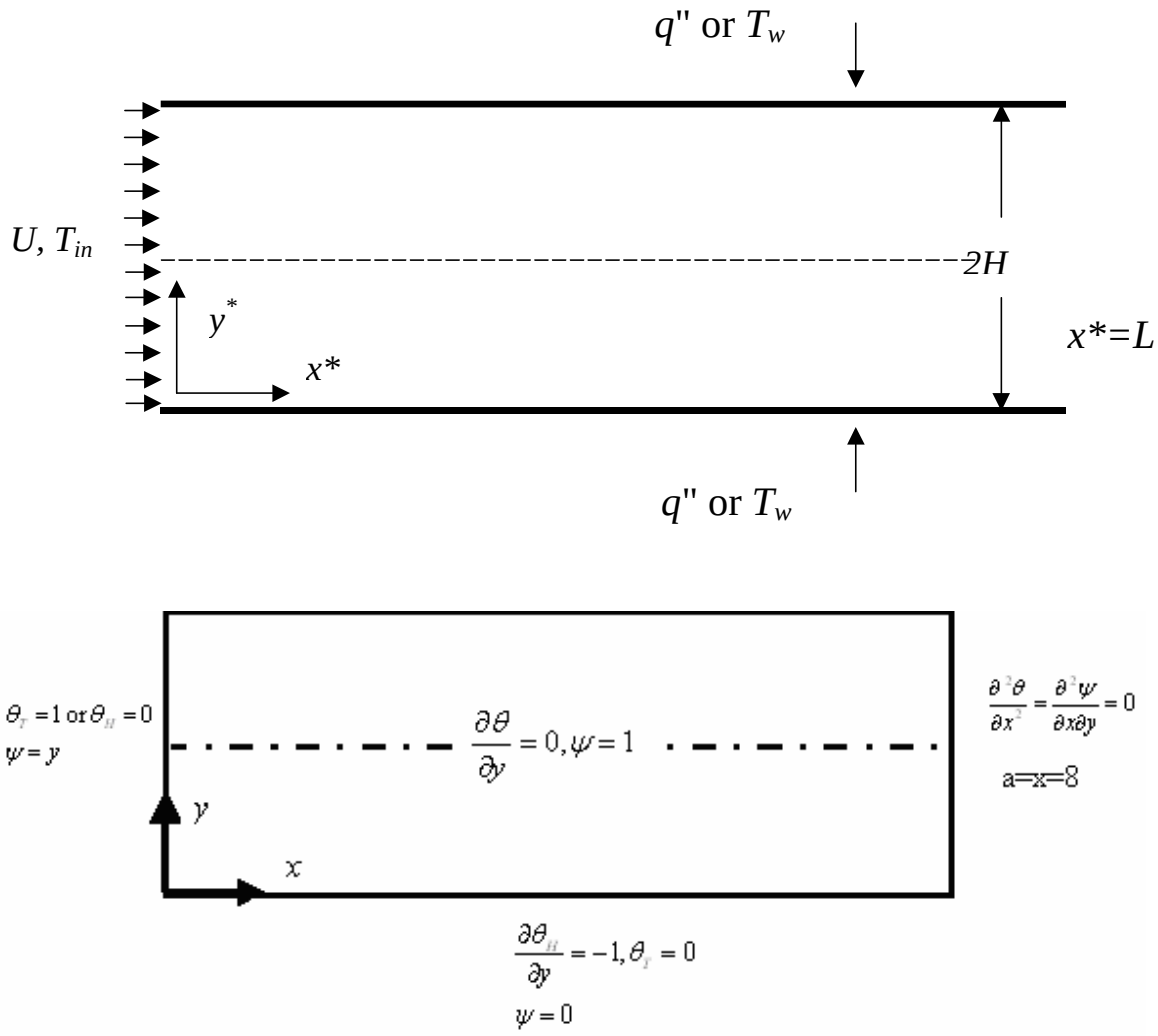

Figure 1-a,b Definition sketch

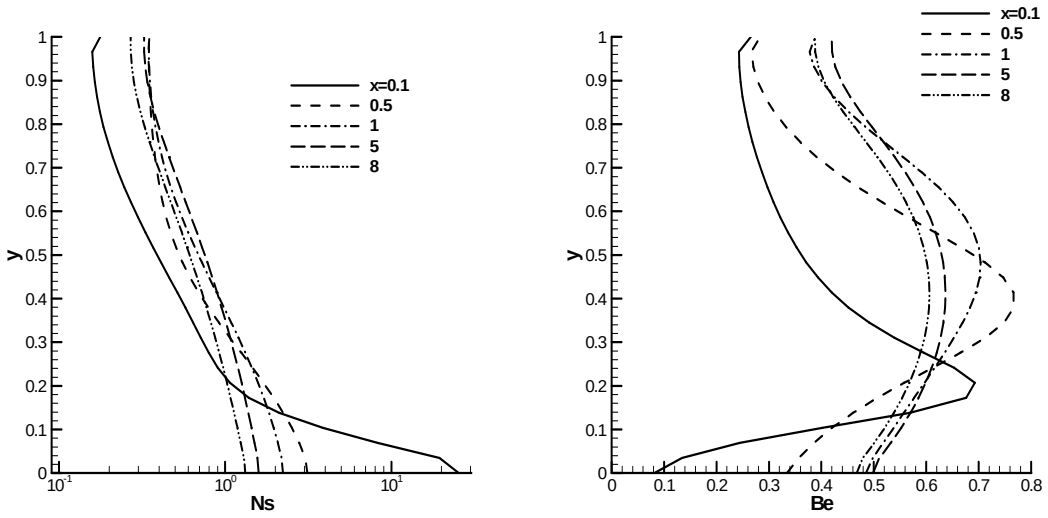

A (S=1) B

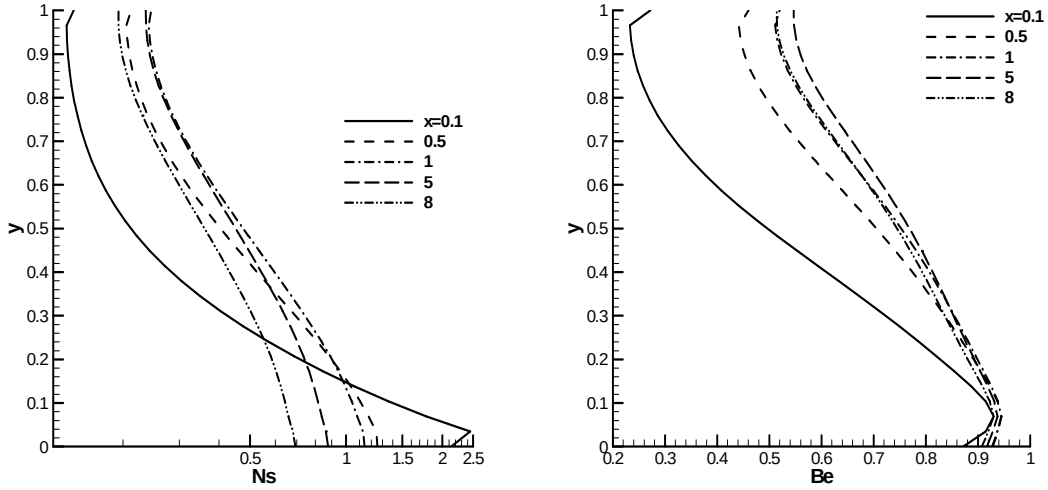

C (S=10) D

Figure 2 Plots of Ns and Be versus y at some streamwise locations (Br*=0.1)

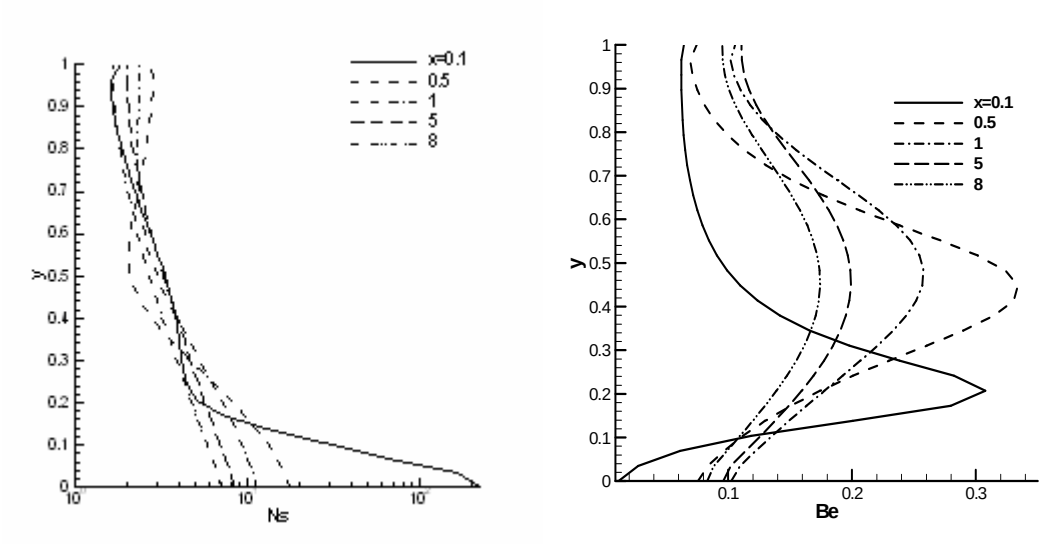

A (S=1) B

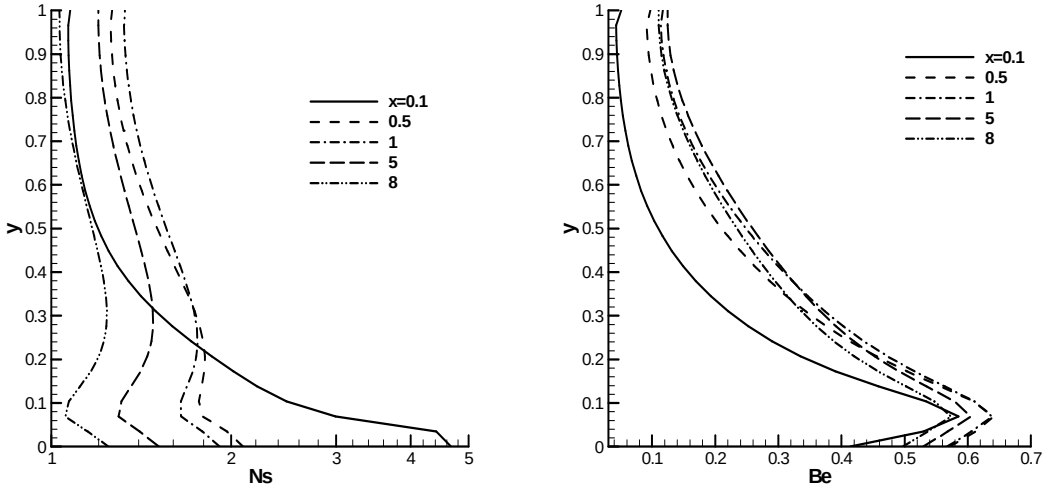

C (S=10) D

Figure 3 Plots of Ns and Be versus y at some streamwise locations (Br*=1)

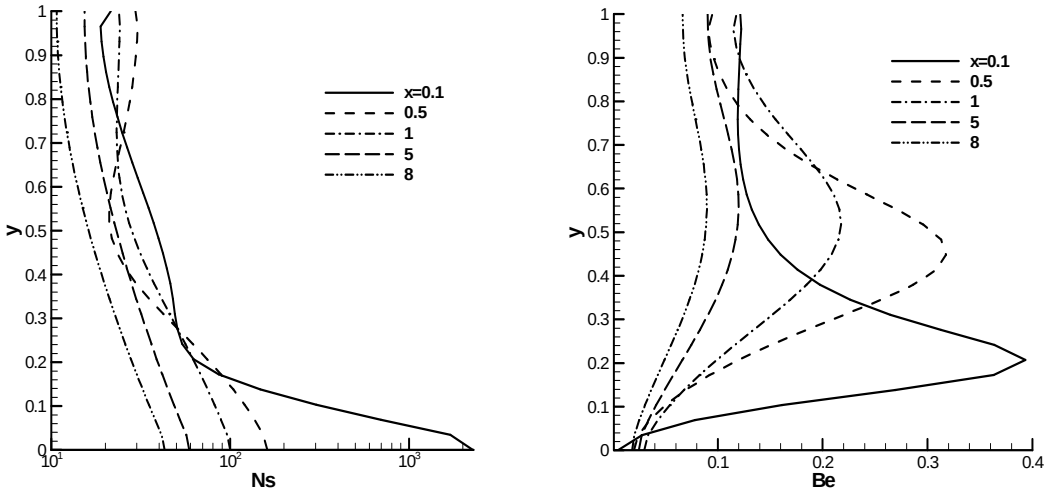

A (S=1) B

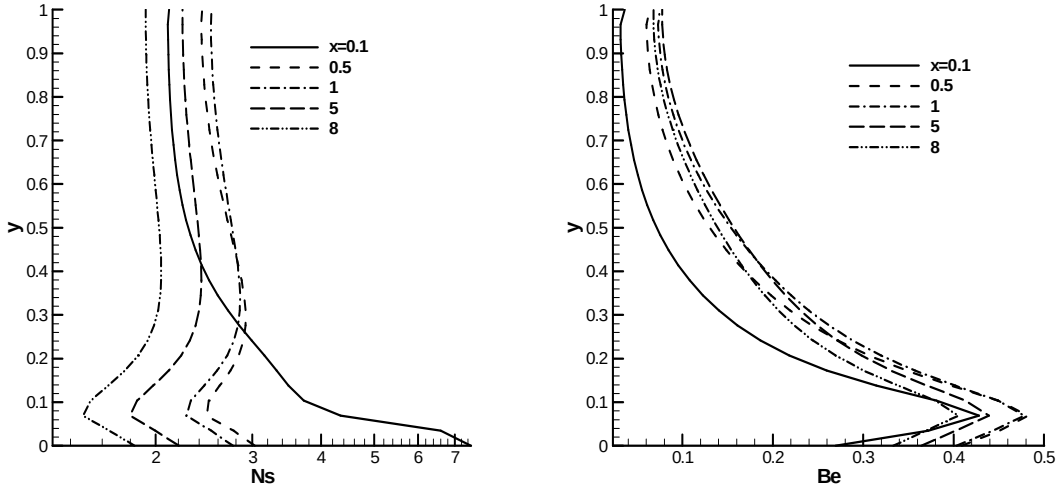

C (S=10) D

Figure 4 Plots of Ns and Be versus y at some streamwise locations (Br*=10)

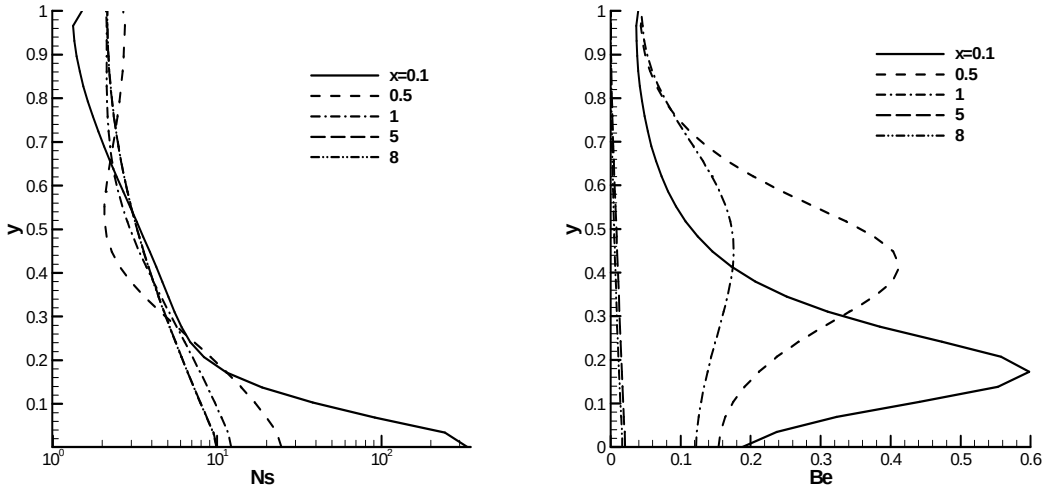

A B

Figure 5 Plots of Ns and Be versus y at some streamwise locations (Br*=1, S=1)

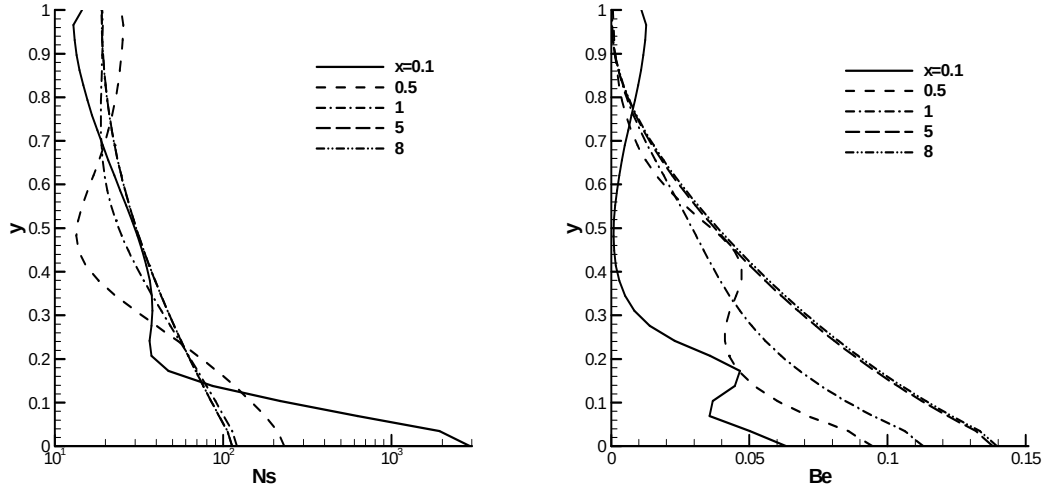

A B

Figure 6 Plots of Ns and Be versus y at some streamwise locations (Br*=10, S=1)

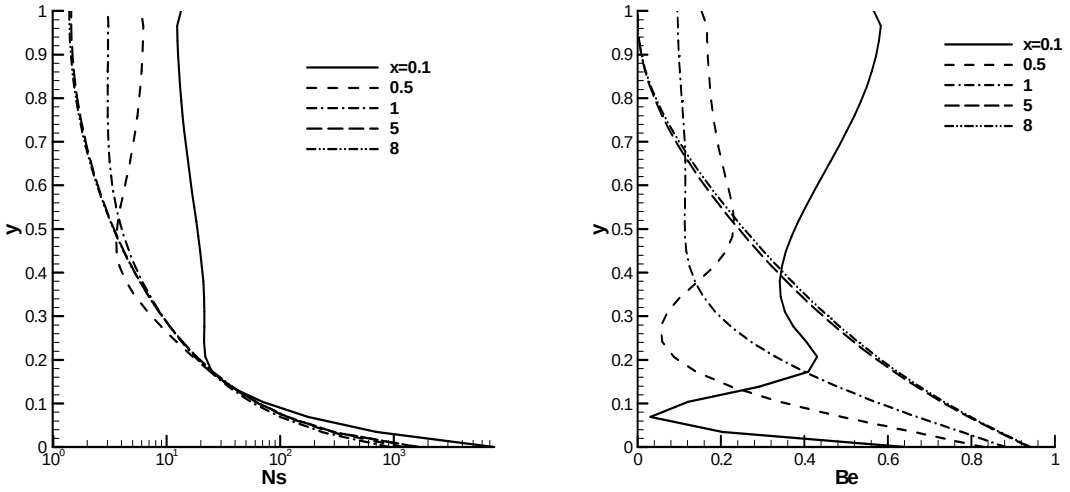

A (S=1) B

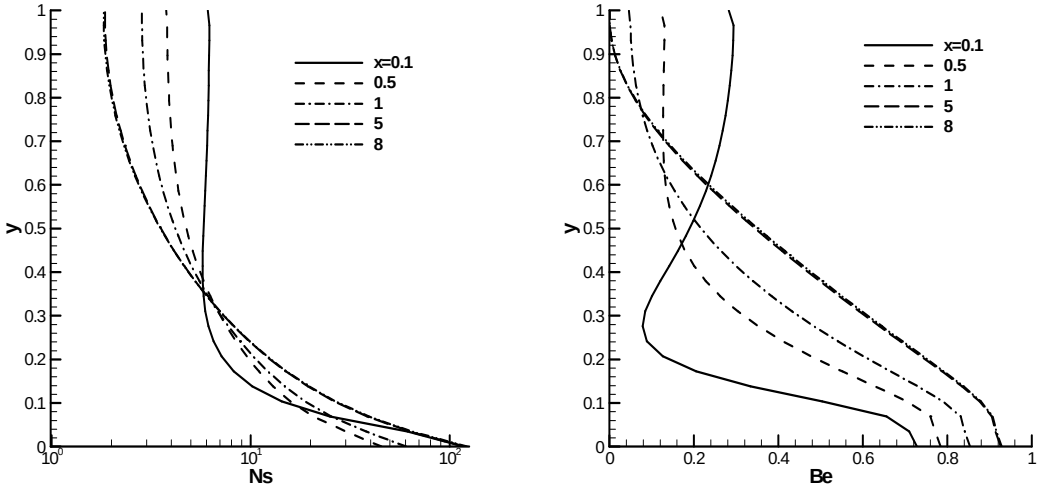

C (S=10) D

Figure 7 Plots of Ns and Be versus y at some streamwise locations (Br*=10, T*=1)

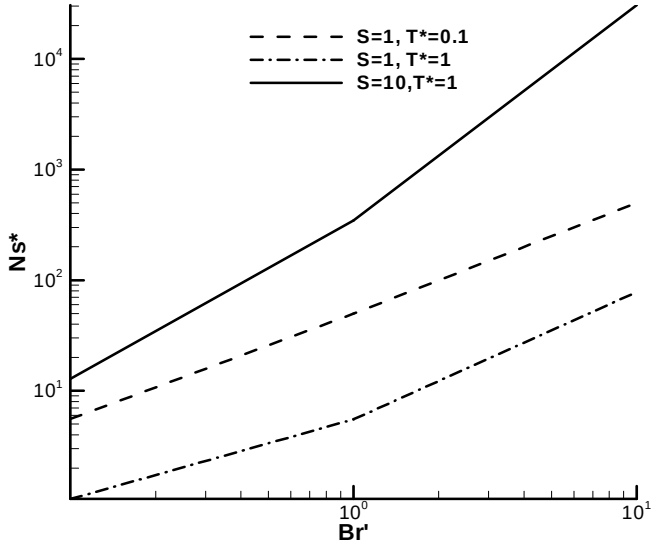

Figure 8 Ns* versus the clear fluid Brinkman number for the **T** boundary condition

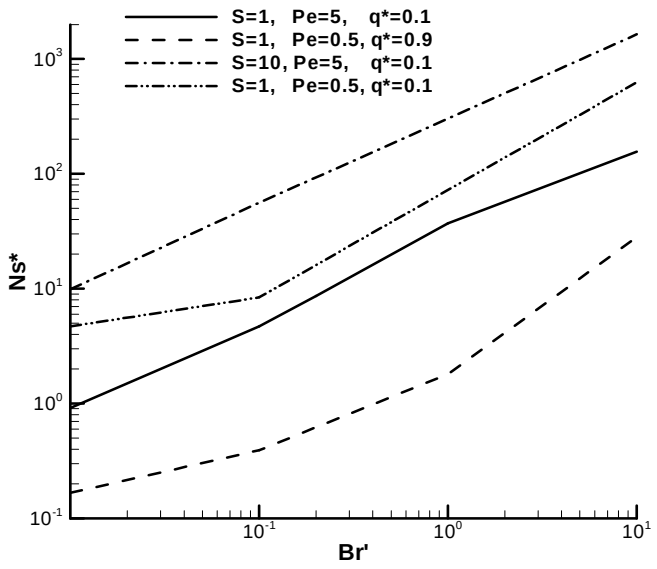

Figure 9 Ns* versus the clear fluid Brinkman number for the **H** boundary condition